Journal of Applied Electrochemistry **31**: 565–572, 2001.

Optimization of hydrogen evolving activity on nickel–phosphorus deposits using experimental strategies

C.-C. HU* and A. BAI
Department of Chemical Engineering, National Chung Cheng University, Chia-Yi, 621 Taiwan
*(*author for correspondence)*

Received 21 February 2000; accepted in revised form 28 November 2000

Key words: electroplating, experimental design, hydrogen evolution, nickel–phosphorus deposits

Abstract

The effects of electroplating variables on the hydrogen evolving activity of Ni–P deposits were systematically examined using fractional factorial design (FFD), path of steepest ascent, and central composite design (CCD) coupled with the response surface method (RSM). The FFD study indicates that the main and interactive effects of temperature, pH, and $NaH_2PO_2 \cdot H_2O$ concentration are the key preparation factors influencing the Ni–P cathode. Empirical models for apparent activity (i), specific activity (i/Ra), and phosphorus content (at %) are fitted against these three variables in the CCD study. These models, represented as contour diagrams, show that a Ni–P deposit with 7 P at % exhibits the maximum electrocatalytic activity.

1. Introduction

Hydrogen is a potential candidate as an efficient and inexpensive energy carrier due to its recyclable and nonpolluting nature [1]. Although hydrogen can easily be produced by the electrolysis of water, this reaction is not very efficient due to the short service-life and/or the high activation overpotential on available cathodes. In addition, the roles of H atoms formed through both underpotential deposition (UPD) and overpotential deposition (OPD) in electrocatalytic hydrogenation are still unclear [2–7] although hydrogen evolution has been extensively investigated [1, 8–12]. A better understanding of electrocatalytic hydrogenation as well as the development of a better electrocatalyst or a longer service-life cathode for hydrogen evolution is very important from both practical and academic points of view.

Although nickel–phosphorus is one of the most promising electrocatalysts for hydrogen evolution in alkaline media [13–15], there are still some conflicting reports concerning its electrocatalytic activity. Shervedani and Lasia [14] proposed that a high H_2 evolving activity of a Ni–P deposit, prepared at a low temperature and a low current density, was attributable to the very high surface area (i.e., a roughness factor of 2000). In contrast, Paseka [13] found that the excellent hydrogen evolving activity of an amorphous Ni–P deposit with 3 wt % phosphorus was due to its intrinsic catalytic activity. Furthermore, Podesta et al. [15] reported that a phosphorus-rich Ni–P deposit (i.e., 25.9 at %) having been heated in air, had a higher activity than that containing a lower phosphorus content (i.e., 12.5 at %). These conflicting observations may be linked to the differences in preparation methods. Thus, a practical, easily controlled and reproducible procedure for preparing Ni–P deposits with optimal activity for hydrogen evolution is required.

A sequential procedure including fractional factorial design (FFD), path of steepest ascent and central composite design (CCD), was employed to achieve statistically significant regression equations modeling the dependence of properties (i.e., hydrogen evolving activity and electrocatalytic activity) on electroplating variables [16–18]. The regression models were then plotted as 'property against variable' contour diagrams, to facilitate straightforward interpretation.

2. Experimental details

Nickel–phosphorus deposits were electroplated onto commercially pure (99.5%) 1 cm × 2 cm Cu plates. These Cu plates were first cleaned with trichloroethylene, rinsed with pure water, and then, anodized at 40 mA cm^{-2} in a 0.1 M NaOH solution for 10 min. After anodizing, the plates were cathodically polarized at 40 mA cm^{-2} in another 0.1 M NaOH solution for 1 min, agitated ultrasonically for 5 min, acid-cleaned with 0.1 M HCl for 2 min, and finally rinsed with pure water. After cleaning, the Cu substrate was placed at the center of a cell between vertical parallel nickel plates of total geometric area 32 cm^2 and electroplated in a typical Watts bath containing 330 g dm^{-3} $NiSO_4 \cdot 6\ H_2O$

(Wako E.P.), 45 g dm^{-3} $NiCl_2$ (Wako E.P.), and 37 g dm^{-3} H_3BO_3 (Tedia E.P.) with pH adjusted with 1 M NaOH and 1 M HCl. The effects of the following electroplating variables on the activity of the Ni–P deposits were investigated in the FFD study: (A) temperature, (B) current density, (C) pH, (D) $NaH_2PO_2.H_2O$ concentration, and (E) stirring rate. Fixed levels of these five variables are given in Table 1. The design matrix with results is shown in Table 2. Electroplating was stopped when the passed charge was 200 C cm^{-2}. The cathodes were then doubly coated with epoxy resin (EP 61, HMH Paint, Japan) leaving an exposed geometric area equal to 1 cm^2. Finally, the epoxy was overlaid with PTFE film when the coatings had hardened.

The average composition of each Ni–P deposit in the CCD design was measured by an energy-dispersive X-ray (EDX) spectroscope at three points using a scanning electron microscope (SEM, Jeol JSM35). X-ray diffraction analysis (XRD: Rigaku X-ray diffractometer using a Cu target) revealed that all Ni–P deposits in the CCD design have an amorphous structure (not shown here).

The apparent activities (i.e., current densities, i) of H_2 evolution of different Ni–P deposits were compared at the same overpotential (i.e., $\eta = -200$ mV in the FFD study and $\eta = -150$ mV in path of steepest ascent and CCD studies) from the Tafel curves. Tafel curves were measured using a pseudo steady-state polarization method with an electrochemical analyser system, BAS-100 W (Bioanalytic System, Inc., USA) in a three-compartment cell. The electrode potentials were first set at −1020 mV ($\eta \approx 0$ mV) for 10 min and then scanned at 0.5 mV s^{-1} to −1250 mV ($\eta \approx -230$ mV). All Tafel curves have been compensated with iR correction (using the positive feedback method) and the log(i)–E curves stabilized after three or four applications of this cathodic polarization. The double-layer capacitance of deposits in the CCD study, employed to evaluate their relative roughness factor (Ra), was measured in 1 M NaOH with an impedance spectrum analyser (IM6, Zahner, Germany) at 0 V d.c. bias with a 10 mV a.c. amplitude. The range of a.c. frequencies used was 50 kHz–1 mHz. Before the impedance measurement, an inert and compact β-$Ni(OH)_2$ film was formed on the deposits by the application of five cycles of CV between 0 and 560 mV at 20 mV s^{-1} in 1 M NaOH. In electrochemical measurements, an Ag/AgCl electrode (Argenthal, 3 M KCl, 207 mV vs SHE at 25 °C) was used as the reference and 4 cm^2 of platinum gauze was employed as the counter electrode. A Luggin capillary, with tip about 1–2 mm from the surface of working electrode, was used to minimize errors due to iR drop in the electrolytes.

Solutions were prepared with pure water produced by a reagent water system (Milli-Q SP, Japan) at 18 MΩ cm. Reagents not specified are Merck, GR. The 1 M NaOH solution was degassed with purified nitrogen gas for 25 min before the electrochemical measurements and a nitrogen blanket was used during the measurements. The temperature of the solution was maintained at 25 °C with an accuracy of 0.1 °C by means of a water thermostat (Haake DC3 and K20).

Table 1. Factors and levels for 2^{5-1} fractional factorial design

Factor		Level	
		−1	1
A	Temperature/°C	20	50
B	Current density/A m^{-2}	500	2500
C	pH	1	4
D	$[NaH_2PO_2]$/M	0.5	1
E	Agitation rate/rpm	200	400

Table 2. The design matrix and experimental data of the hydrogen evolving activity at $\eta \approx -200$ mV for 2^{5-1} fractional factorial design with the defining relation I = ABCDE

Run	Factor					i/mA cm^{-2} (η = −200 mV)
	A	B	C	D	E	
1	−1	−1	−1	−1	1	17
2	1	−1	−1	−1	−1	3.0
3	−1	1	−1	−1	−1	1.1
4	1	1	−1	−1	1	4.9
5	−1	−1	1	−1	−1	43
6	1	−1	1	−1	1	71
7	−1	1	1	−1	1	71
8	1	1	1	−1	−1	43
9	−1	−1	−1	1	−1	18
10	1	−1	−1	1	1	0.8
11	−1	1	−1	1	1	1.5
12	1	1	−1	1	−1	122
13	−1	−1	1	1	1	11
14	1	−1	1	1	−1	189
15	−1	1	1	1	−1	0.3
16	1	1	1	1	1	99

3. Results and discussion

3.1. *Fractional factorial design*

The fractional factorial design (FFD) method was employed to identify the key electroplating variables. This allows the influence of each preparation variable to be observed at a variety of other variable levels, as well as interactions among the variables.

The observations of activity of Ni–P cathodes at an overpotential of −200 mV, with the design matrix in the 2^{5-1} FFD experiments are shown in Table 2. According to the defining relation I=ABCDE [16, 18], the combination of observations used to estimate the effect of the main factor E (agitation rate) is identical to that used to estimate the four-factor interaction effect of the aliases A (temperature), B (current density), C (pH) and D ($NaH_2PO_2 \cdot H_2O$ concentration) [16, 18]. From the principle of the sparsity of effects [18], a system is likely to be driven primarily by main factor and low-order interaction effects. Effects of the high-order (e.g., three

and greater order) interactions are assumed to be negligible. Thus, the effect of A × B × C × D interaction can be ignored enabling the effect of the main factor E to be isolated. Factors A to D are determined similarly.

The observations presented in Table 2, were subjected to regression analysis according to the method of Montgomery [18] and the analysis of variance (ANOVA) of i is summarized in Table 3. The statistics test factor, F, is defined as $F = \mathrm{MSF/MSE}$, where MSF and MSE are the mean squares of factors or interactions and mean squares of errors, respectively. If the calculated value of F is greater than the F in the table at a specified probability level (e.g., $F_{0.05}(1, 5) = 6.61$), a statistically significant factor or interaction is obtained. After the test, factors A, C, D and E, interactions A × C, A × D, A × E, B × C, B × E and D × E have statistically significant effects on the activity of Ni–P cathodes, indicating the complicated influences of the preparation variables. The multiple correlation coefficient, R^2, defined as $R^2 = (\mathrm{SST} - \mathrm{SSE})/\mathrm{SST} = 1 - (\mathrm{SSE/SST})$, represents the proportion of SST (sum of squares of total variances) explained by the fitted equation. An R^2 value close to 1 means a good fit to the experimental data ($R^2 = 0.9823$ in this model).

From a combination of the estimates of the experimental variable effects and the ANOVA results, a fitted polynomial model with statistical significance can be generated:

$$\begin{aligned} i = {} & 43.54 + 23.09\,x_{\mathrm{A}} + 22.40\,x_{\mathrm{C}} + 11.72\,x_{\mathrm{D}} - 8.92\,x_{\mathrm{E}} \\ & + 11.50\,x_{\mathrm{A}}x_{\mathrm{C}} + 24.25\,x_{\mathrm{A}}x_{\mathrm{D}} - 13.75\,x_{\mathrm{A}}x_{\mathrm{E}} \\ & - 12.00\,x_{\mathrm{B}}x_{\mathrm{C}} + 10.05\,x_{\mathrm{B}}x_{\mathrm{E}} - 18.20\,x_{\mathrm{D}}x_{\mathrm{E}} \end{aligned} \quad (1)$$

where x_i are the coded variables for factors i (i.e., A, B, C, D and E). The coded variables, x_i, are defined in a standardized form as follows [18, 21]:

$$x_{i,\mathrm{HIGH}} = (X_{i,\mathrm{HIGH}} - X_{i,\mathrm{MEAN}})/S_i \quad (= +1) \quad (2)$$

$$x_{i,\mathrm{LOW}} = (X_{i,\mathrm{LOW}} - X_{i,\mathrm{MEAN}})/S_i \quad (= -1) \quad (3)$$

Table 3. Analysis of variance for the hydrogen evolving activity from 2^{5-1} fractional factorial design

Source	d.f.	SS	MS	F
A	1	8526	8526	73.88
C	1	8027	8027	69.59
D	1	2200	2200	19.06
E	1	1273	1273	11.03
AC	1	2120	2120	18.37
AD	1	9439	9439	81.79
AE	1	3014	3014	26.12
BC	1	2297	2297	19.90
BE	1	1616	1616	14.00
DE	1	5299	5299	45.92
Error	5	778	115.4	
Total	15	44593		

$R^2 = 0.9823$.

$$X_{i,\mathrm{MEAN}} = (X_{i,\mathrm{LOW}} + X_{i,\mathrm{HIGH}})/2 \quad (4)$$

$$S_i = (X_{i,\mathrm{HIGH}} - X_{i,\mathrm{LOW}})/2 \quad (5)$$

where $X_{i,\ \mathrm{HIGH}}$ and $X_{\mathrm{i},\ \mathrm{LOW}}$, respectively, represent the high and low levels of factor i in natural units (e.g., °C, A dm^{-2}, etc.).

The effects of factors A to E and two-factor interactions with statistical significance on the activity of the Ni–P deposit are shown in Figure 1(a) and (b), respectively. Figure 1(a) shows a sharp increase from about 20 to 67 mA cm^{-2} and from about 22 to 65 mA cm^{-2} with increasing temperature and pH of the baths, respectively. These results are also supported by the ANOVA statistical test in Table 3 in which factors A (temperature) and C (pH) are the most important preparation variables affecting the activity of Ni–P cathodes. In Figure 1(b), the effect of temperature (factor A) is greater at higher pH (the high level of factor C) or a lower agitation rate (the low level of factor E). Furthermore, the effect of temperature (factor A) is positive at a higher concentration of $NaH_2PO_2 \cdot H_2O$ (the high level of factor D) while a negative effect is found at a lower concentration (the low level of factor D). These trends indicate A × C, A × D and A × E interactions. A

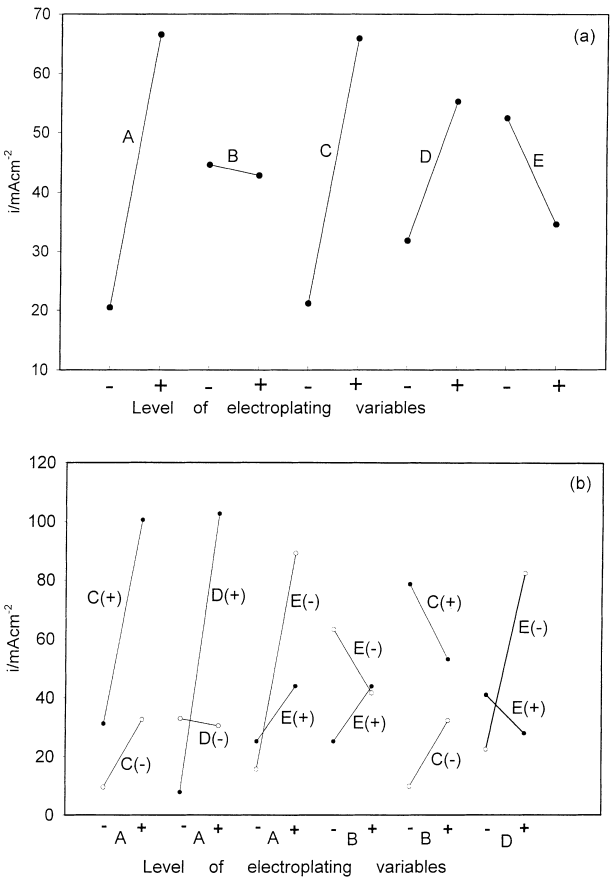

Fig. 1. (a) Main effects of electroplating temperature (A), electroplating current density (B), pH (C), $NaH_2PO_2 \cdot H_2O$ concentration (D), and agitation rate (E) on the H_2 evolving activity of Ni–P deposits. (b) Effects of two-factor interactions with statistical significance; where (+) and (–) indicate the high and low levels of factors, respectively.

similar situation is also found for the B × C, B × E and D × E interactions.

Figure 1(b) indicates the complicated influences of A × C, A × D, A × E, B × C, B × E and D × E interactions. Conflicting conclusions on the H_2 evolving activity of Ni–P cathodes have been drawn by different researchers since interactions between electroplating variables are difficult to identify from experiments testing one factor at a time. For example, Shervedani and Lasia [14] proposed that Ni–P deposits prepared at low temperatures and low electroplating current densities, exhibited high H_2 evolving activities. However, in Figure 1(a), the activity of a Ni–P cathode is sharply enhanced by an increase in temperature (factor A) but the current density (factor B) is demonstrated to be an insignificant factor. Due to the complicated influences of A × C, A × D, A × E, B × C and B × E interactions, optimization of the Ni–P cathode is readily achieved by the sequential procedure of experimental design.

3.2. *Paths of steepest ascent*

In the previous section, factors A (temperature), C (pH), D ($NaH_2PO_2 \cdot H_2O$ concentration), E (agitation rate) and A × C, A × D, A × E, B × C, B × E and D × E interactions are determined to be the key variables influencing the activity of Ni–P deposits. The effects of these variables are further verified in the study of the path of steepest ascent. The existence of synergism between factors and interactions is favoured when the electroplating variables are moved simultaneously in the direction of steepest ascent. If this situation cannot be satisfied, a compromise in changing these variables should be affected. According to Figure 1(a), the direction of steepest ascent (based on main effects of factors) should be A+ (increasing temperature), C+ (increasing pH), D+ (increasing $NaH_2PO_2 \cdot H_2O$ concentration), and E− (decreasing agitation rate). Fortunately, Figure 1(b) shows that synergistic effects can also be obtained when factor E is moved in the negative direction and factors A, C and D are moved simultaneously in the positive directions. The current density has to be fixed at a low level (500 A m^{-2}) in order to obtain synergism in B × C and B × E interactions.

According to the steepest ascent methodology [17], the electroplating variables are simultaneously moved to $+23.09\ S_A$, $+22.40\ S_C$, and $+11.72\ S_D$ in x_A, x_C and x_D directions, respectively, for every $-8.92\ S_E$ in the x_E direction (i.e., ratio of step size ≈ 1:1:0.5:0.3). Typical points on the path of steepest ascent are shown in Table 4, which indicates that the maximum apparent activity (i.e., current density) of H_2 evolution is located near the experimental settings of run 2. Accordingly, the experimental settings of run 2 in Table 4 should be employed as the center point in the CCD study. However, a model checking for the quadratic terms has to be applied before the employment of the full central composite design. The design matrix and experimental results for the model checking are listed in Table 5. Factor *E* is ignored since the calculated *F* value of factor *E* indicates it has less significance than the others from the regression analysis (see Table 3). From Table 5, a new direction for the second path of steepest ascent is deduced. Typical points on the second path of steepest ascent are shown in Table 6. These results indicate that the maximum current density for the HER should be located near the experimental settings of run 2 in Table 6 although there are two maxima in these experiments. Hence, the experimental settings of run 2 in Table 6 are employed as the central point settings in the CCD study. A model checking for the quadratic terms also has to be applied before undertaking the full CCD experiment. Fortunately, a statistically significant model with quadratic terms is obtained in this case.

Table 4. Points on the first path of steepest ascent ($\eta \approx -150$ mV)

Run	Factor				i/mA cm^{-2} ($\eta = -150$ mV)
	A	C	D	E	
1	35	2.5	0.75	300	68
2	50	4.0	0.875	250	129
3	65	5.5	1	200	29

Table 5. Design matrix and experimental data of the hydrogen evolving activity, measured at $\eta \approx -150$ mV, in checking the model for a central composite design with a quadratic form fit

Run	Factor			i/mA cm^{-2} ($\eta = -150$ mV)
	A	C	D	
1	42	5	0.938	108
2	42	3	0.938	74
3	42	5	0.812	120
4	42	3	0.812	87
5	58	5	0.938	62
6	58	3	0.938	42
7	58	5	0.812	124
8	58	3	0.812	135
9	50	4	0.875	128, 128, 128

Table 6. Points on the second path of steepest ascent ($\eta \approx -150$ mV)

Run	Factor			i/mA cm^{-2} ($\eta = -150$ mV)
	A	C	D	
1	50	4	0.875	128
2	46.3	3.6	0.849	152
3	42.5	3.1	0.823	98
4	38.7	2.7	0.796	84
5	35	2.2	0.770	107
6	31.2	1.8	0.744	47

Table 7. Factors and levels for the central composite design

Level	Factor		
	A	C	D
$-\sqrt{3}$	37.3	3.0	0.756
−1	41	3.2	0.795
0	46	3.5	0.849
1	51	3.8	0.903
$\sqrt{3}$	54.7	4.0	0.942

3.3. *Central composite design*

To find the optimal experimental settings for preparing Ni–P, further verification of the influences of the key factors in the vicinity of the experimental settings of run 2 in Table 6 was undertaken. The design factors and levels for the 17 experiments in the CCD study are shown in Table 7. The results of apparent activity of H_2 evolution (i), double-layer capacitance (C_{dl}), specific activity (i/Ra) of H_2 evolution and the atomic percent of phosphorus (P at %) within the deposits are listed together with the design matrix in Table 8. In this Table, three repeats at the original point were performed in order to evaluate the pure error of experiments.

The activity of hydrogen evolution on a Ni–P cathode, predominantly governed by both the real surface area and the specific activity of electrocatalysts, is usually evaluated through comparisons of current density (i) at a constant overpotential. On the other hand, the investigation of electrocatalytic effects is also important. In order to identify the true electrocatalytic effects of Ni–P deposits, comparisons must be carried out for the same real surface area. Since the capacitance of the electrical double layer, C_{dl}, is directly proportional to the real surface area [19, 20], a relative roughness factor (Ra), calculated from Equation 6 is believed to represent the relative surface area of a Ni–P cathode.

$$Ra(\text{relative roughness factor}) = C_{dl}/20(\mu\text{F cm}^{-2}) \quad (6)$$

Double-layer capacitance was measured by the a.c.-impedance spectroscopy at 0 V after application of five cycles of CV between 0 and 560 mV, thereby ensuring the complete formation of a compact and passive layer of β-$Ni(OH)_2$ on the deposit to avoid the redox transitions of nickel hydroxide in different oxidation states. Thus, the contribution of pseudocapacitance resulting from the redox transitions of oxyhydroxylnickel species is negligible and the relative surface area of Ni–P cathodes can be obtained. Hence, i/Ra actually represents the normalized activity.

The results of apparent activity (i), specific (electrocatalytic) activity (i/Ra) and P at % shown in Table 8, were subjected to regression analysis, and generated the following equations.

$$i = 159.81 - 7.21x_A + 2.67x_D - 11.38x_A^2 - 6.79x_C^2 - 6.48x_D^2 - 3.64x_Cx_D \quad (7)$$

$$i/Ra = 26.32 - 1.54x_A^2 - 1.33x_C^2 - 1.52x_D^2 \quad (8)$$

$$\text{P(at \%)} = 6.89 + 0.31x_A - 0.22x_C + 0.65x_A^2 + 0.49x_C^2 + 0.46x_D^2 \quad (9)$$

where x_A, x_C and x_D, respectively, represent the coded variables of factors A, C and D. The magnitudes of coefficients in the regression equation illustrate the relative effects of linear, quadratic, and interactions for factors A (temperature), C (pH) and D ($NaH_2PO_2 \cdot H_2O$ concentration) in the electroplating solution on the

Table 8. Design matrix and experimental data of activity (i measured at $\eta \approx -150$ mV) and specific activity (i/Ra) of hydrogen evolution, double-layer capacitance, and P (at %) in Ni–P deposits in the central composite design with a quadratic form fit

Run	Factor			i/mA cm^{-2} η = −150 mV	C_{dl}/μF cm^{-2}	Specific activity	P at %
	A	C	D				
1	−1	1	1	151	140.6	21.5	7.6
2	−1	−1	1	144	128.2	22.5	8.4
3	−1	1	−1	132	118.7	22.3	7.5
4	−1	−1	−1	142	126.9	22.4	9.2
5	1	1	1	123	111.5	22.1	8.7
6	1	−1	1	121	111.8	21.6	8.9
7	1	1	−1	129	119.6	21.6	8.2
8	1	−1	−1	123	109.4	22.5	9.0
9	$\sqrt{3}$	0	0	120	109.2	22.0	9.6
10	$-\sqrt{3}$	0	0	136	129.6	21.1	8.3
11	0	$\sqrt{3}$	0	149	134.2	22.2	8.6
12	0	$-\sqrt{3}$	0	135	122.2	22.1	8.3
13	0	0	$\sqrt{3}$	150	135.3	22.2	8.3
14	0	0	$-\sqrt{3}$	136	129.3	21.0	8.5
15	0	0	0	159	120.5	26.4	6.8
16	0	0	0	159	121.5	26.2	7.0
17	0	0	0	161	122.2	26.4	6.9

properties of interest. Terms without statistical significance were deleted from the full second-order model from the analysis of variance for every regression coefficient.

All ANOVA data show that the regressed Equations 7–9 are 'statistically significant' since the calculated values of the test statistics, F (=15.93, 75.37 and 10.68 for Equations 7–9, respectively), are much larger than those of F in the Table at a specified probability level (e.g., $F_{0.05}(5, 11)=3.20$). The R^2 values of Equations 7, 8 and 9 are 0.917, 0.946 and 0.829, respectively. Since the value of R^2 (0.829) for Equation 9 is relatively lower, this regression model is considered to be a fair representation of the dependence of P content on factors A, C and D. The relatively poor representation of phosphorus content by Equation 9 is attributable to the intrinsic inaccuracy (~0.5 at %) of EDX, which rendered a relatively larger proportion of unexplained variance. Therefore, only Equations 7 and 8 accurately represent the dependence of the apparent activity and specific activity of Ni–P cathodes for hydrogen evolution on factors A, C and D in the CCD study.

3.4. *Contour plots*

Regression Equations 7 and 8 were used in constructing the contour plots for apparent activity (i) and specific activity (i/Ra) against temperature (A), pH (C), and $NaH_2PO_2 \cdot H_2O$ concentration (D) in the electroplating bath, shown in Figures 2 and 3, respectively. These contour diagrams facilitate a direct examination of the dependence of these response properties on the electroplating variables. The coordinates, x, y and z in these diagrams, respectively, indicate factors A, C and D. In addition, z ranges from 0 to 1 in Figures 2(a) and 3(a) while it ranges from 0 to −1 in Figures 2(b) and 3(b).

Figure 2 shows that contour plots of the H_2 evolving activity (apparent current density) form distorted semispherical shells with their centers located at about $x = -0.30$, $y = -0.33$ and $z = +0.50$. The extreme region with maximum values of i ($\geq$159 mA cm^{-2}) occurs within the circle labeled 159. Within this circle, the temperature, pH, and $NaH_2PO_2 \cdot H_2O$ concentration of the deposition baths range from about 47 to 42 °C, from about 3.4 to 3.7, and from about 0.84 to 0.91 M, respectively. In addition, a Ni–P cathode electroplated from the baths with a temperature of 44.5 °C, pH of 3.55 and a $NaH_2PO_2 \cdot H_2O$ concentration of 0.875 M is expected to exhibit the maximum activity (>159 mA cm^{-2}) for the HER. This prediction was confirmed and the current density of H_2 evolution on this cathode was 162.8 mA cm^{-2} at an overpotential of −150 mV. Therefore, the regression models proposed are significant and acceptable.

In Figure 3, the contour plots for specific activity of H_2 evolution form very symmetrical hemispherical shells with their centers located at the origin since there are neither interactions nor linear terms in Equation 8. Thus, a maximum in specific (electrocatalytic) activity of hydrogen evolution should be obtained on the cathode electroplated in the bath at 46 °C, pH of 3.5 and a $NaH_2PO_2 \cdot H_2O$ concentration of 0.85 M, respectively. The extreme region with a maximum of i/Ra ($\geq$26) occurs within the circle marked 26. Within this circle, temperature, pH, and $NaH_2PO_2 \cdot H_2O$ concentration of the bath, respectively, range from about 48.5 to 43.5 °C, from about 3.35 to 3.65, and from about 0.82 to 0.88 M. From a comparison of i/Ra and P (at %) data in Table 8, a deposit with the minimum phosphorus content exhibits the maximum specific activity of hydrogen evolution. In addition, there is possibly a negative dependence of electrocatalytic activity of hydrogen evolution on the phosphorus content.

Amongst several studies of Ni–P cathodes for hydrogen evolution [13–15], conflicting conclusions were found. In this work, a Ni–P deposit with ~7 at % phosphorus (~3.8 wt % P) exhibits the maximum

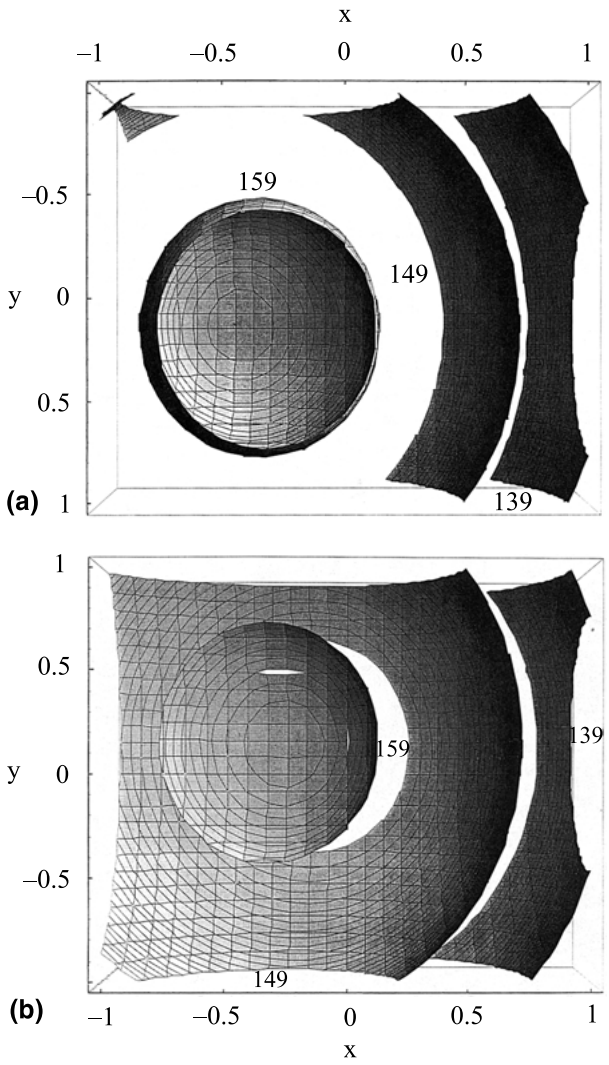

Fig. 2. Contour plots for constant hydrogen evolving activity (i) of the Ni–P deposits at $\eta \approx -150$ mV vs the electroplating temperature (x), pH (y), and $NaH_2PO_2 \cdot H_2O$ concentration (z) in the electroplating baths; (a) $z = [0, 1]$ and (b) $z = [0, -1]$.

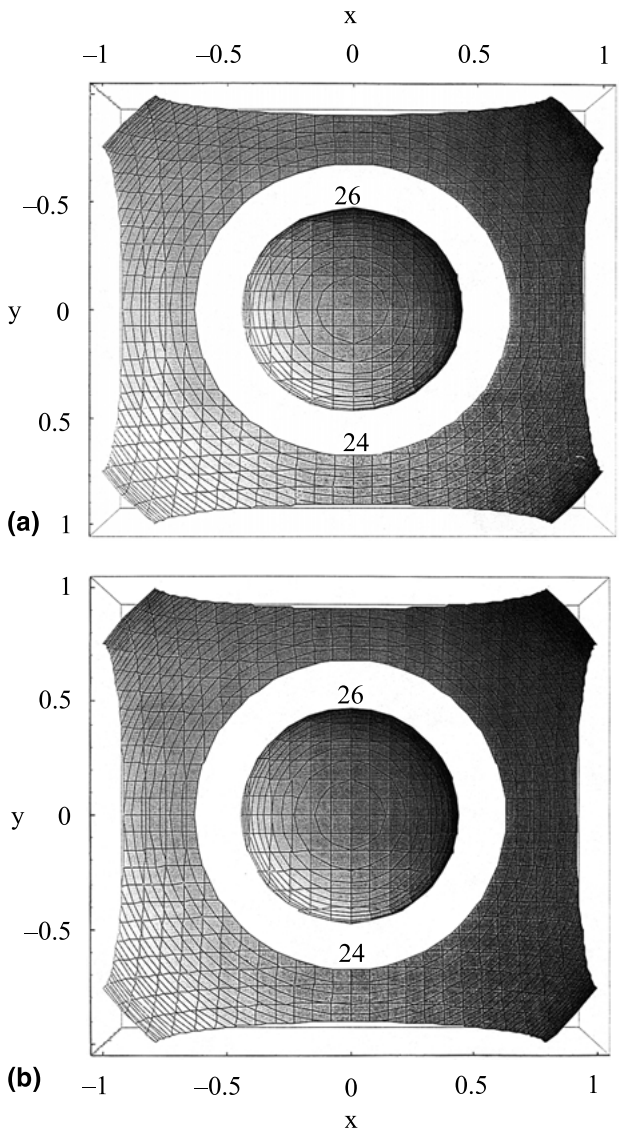

Fig. 3. Contour plots for specific activity (i/Ra) of the Ni–P deposits for hydrogen evolution vs the electroplating temperature (x), pH (y), and $NaH_2PO_2 \cdot H_2O$ concentration (z) in the electroplating baths; (a) $z = [0, 1]$ and (b) $z = [0, -1]$.

electrocatalytic activity (i.e., i/Ra) for hydrogen evolution. This composition is very close to the results reported by Paseka [13] and by as Shervedani and Lasia [14]. However, the excellent hydrogen evolving activity of this Ni–P cathode is attributable to its intrinsic electrocatalytic activity (similar to that reported by Paseka [13]). This is further supported by the fact that the relative roughness factor (Ra) of all deposits in the CCD study only varies from about 5.5 to 7 although the real roughness factor of these cathodes should be several times (e.g., 10 times) Ra. The effects of real surface area on the apparent activity of these cathodes are thus considered not to be as important as proposed by Shervedani and Lasia (i.e., $Ra = 2000$) [14]. In our opinion, a roughness factor of 2000 for the Ni–P deposits prepared at a very low current density [14] is doubtful because their surfaces should be relatively smooth and compact in nature [21]. This speculation is also confirmed by an examination of their SEM photographs. The reasons for the over-estimation of surface roughness of the Ni–P deposits are still unclear. One possible reason may be the contribution of pseudocapacitance of OPD H atoms or absorbed H atoms generated by the low frequency arc (reported in that work), when capacitance was measured at relatively high overpotentials of hydrogen evolution. If this is the case, capacitance of the electrical double layer, measured by the AC-impedance method at 0 V in 1 M NaOH for the deposit with 5 CV cycles between 0 and 560 mV at 20 mV s^{-1}, can be used to evaluate the real surface areas of Ni–P deposits, if the exact C_{dl} value of a passive, compact, smooth, and flat β-$Ni(OH)_2$ film is measured.

4. Conclusions

Using the sequential experiment strategies (i.e., fractional factorial design, paths of steepest ascent, and central composite design coupled with the response surface method), the H_2 evolving activity of the electroplated Ni–P cathode is predominantly determined by the main and interactive effects of temperature, pH, and $NaH_2PO_2 \cdot H_2O$ concentration. A Ni–P cathode with the highest hydrogen evolving activity ($i \geq 159$ mA cm^{-2}) is electroplated in the baths with temperatures from 47 to 42 °C, pH from 3.4 to 3.7, and $NaH_2PO_2 \cdot H_2O$ concentrations from 0.84 to 0.91 M, respectively. A Ni–P deposit with the minimum P content (i.e., 7 at % $\approx$ 3.8 wt %) in the CCD study, electroplated in the bath with a temperature of 46 °C, pH of 3.5 and a $NaH_2PO_2 \cdot H_2O$ concentration of 0.85 M, exhibits the maximum specific activity for the HER. The intrinsic electrocatalytic activity of Ni–P is the predominant factor promoting the H_2 evolving activity.

Acknowledgements

Financial support of this work, by the National Science Council of the Republic of China under contract NSC 89-2214-E-194-008, is gratefully acknowledged.

References

1. C.-C. Hu and C.-Y. Weng, *J. Appl. Electrochem.* **30** (2000) 499.
2. C.-C. Hu and T.-C. Wen, *Electrochim. Acta* **43** (1998) 1747.
3. C.-C. Hu and T.-C. Wen, *J. Electrochem. Soc.* **142** (1995) 1376.
4. K. Park, P.N. Pintauro, M.M. Baizer and K. Nobe, *J. Appl. Electrochem.* **16** (1986) 941.
5. M.J. Lain and D. Pletcher, *Electrochim. Acta* **32** (1987) 109.
6. S.J.C. Cleghorn and D. Pletcher, *Electrochim. Acta* **38** (1993) 425.
7. V. Anantharaman and P.N. Pintauro, *J. Electrochem. Soc.* **141** (1994) 1376 and 2742.
8. T.-C. Wen, S.-M. Lin and T.-M. Tsai, *J. Appl. Electrochem.* **24** (1994) 233.
9. D. Los, A. Rami and A. Lasia, *J. Appl. Electrochem.* **23** (1993) 135.
10. C.-C. Hu, C.-Y. Lin and T.-C. Wen, *Mat. Chem. Phys.* **44** (1996) 233.

11. R. Kötz and S. Stucki, *J. Appl. Electrochem.* **17** (1987) 1190.
12. T.-C. Wen and C.-C. Hu, *J. Electrochem. Soc.* **139** (1992) 2158.
13. I. Paseka, *Electrochim. Acta* **44** (1999) 4551.
14. R.K. Shervedani and A. Lasia, *J. Electrochem. Soc.* **144** (1997) 511.
15. J.J. Podesta, R.C.V. Piatti, A.J. Arvia, P. Ekundge, K. Juttner and G. Kreysa, *Int. J. Hydrogen Energy* **17** (1992) 9.
16. G.E.P. Box, W.G. Hunter and J.S. Hunter, 'Statistics for Experiments', (J. Wiley & Sons, New York, 1978), p. 374.
17. J.A. Cornell, 'How to Apply Response Surface Methodology', Vol. 8 (ASQC, Wisconsin, 1990).
18. D.C. Montgomery, 'Design and Analysis of Experiments', 4th edn (J. Wiley & Sons, Singapore, 1997).
19. A.J. Bard and L.R. Faulkner, 'Electrochemical Methods, Fundamentals and Applications' (J. Wiley & Sons, Singapore, 1980), p. 8.
20. R.L. McCreery and K.K. Cline, *in* P.T. Kissinger and W.R. Heineman (Eds), 'Laboratory Techniques in Electroanalytical Chemistry' (Marcel Dekker, Hong Kong, 1996), p. 295.
21. D. Pletcher and F.C. Walsh, 'Industrial Electrochemistry', 2nd edn (Chapman & Hall, New York, 1990), p. 395.